SCIENCE CHINA
Physics, Mechanics & Astronomy

• Article •
Editor's Focus

January 2021 Vol. 64 No. 1: 217062
https://doi.org/10.1007/s11433-020-1597-6

Editor's Focus

Spin excitations and spin wave gap in the ferromagnetic Weyl semimetal $Co_3Sn_2S_2$

Chang Liu[1,2†], JianLei Shen[1,2†], JiaCheng Gao[1,2†], ChangJiang Yi[1,2], Di Liu[1,2], Tao Xie[1,2], Lin Yang[1,2], Sergey Danilkin[3], GuoChu Deng[3], WenHong Wang[1,4], ShiLiang Li[1,2,4], YouGuo Shi[1,2,4,5], HongMing Weng[1,2,4,5*], EnKe Liu[1,4*], and HuiQian Luo[1,4*]

[1]*Beijing National Laboratory for Condensed Matter Physics, Institute of Physics, Chinese Academy of Sciences, Beijing 100190, China;*
[2]*School of Physical Sciences, University of Chinese Academy of Sciences, Beijing 100190, China;*
[3]*Australian Centre for Neutron Scattering, Australian Nuclear Science and Technology Organization, Lucas Heights NSW-2234, Australia;*
[4]*Songshan Lake Materials Laboratory, Dongguan 523808, China;*
[5]*Physical Science Laboratory, Huairou National Comprehensive Science Center, Beijing 101407, China*

Received May 31, 2020; accepted June 24, 2020; published online August 13, 2020

We report a comprehensive neutron scattering study on the spin excitations in the magnetic Weyl semimetal $Co_3Sn_2S_2$ with a quasi-two-dimensional structure. Both in-plane and out-of-plane dispersions of the spin waves were revealed in the ferromagnetic state. Similarly, dispersive but damped spin excitations were found in the paramagnetic state. The effective exchange interactions were estimated using a semi-classical Heisenberg model to consistently reproduce the experimental T_C and spin stiffness. However, a full spin wave gap below $E_g = 2.3$ meV was observed at $T = 4$ K. This value was considerably larger than the estimated magnetic anisotropy energy (~0.6 meV), and its temperature dependence indicated a significant contribution from the Weyl fermions. These results suggest that $Co_3Sn_2S_2$ is a three-dimensional correlated system with a large spin stiffness, and the low-energy spin dynamics can interplay with the topological electron states.

magnetic Weyl semimetal, topological materials, spin excitations, neutron scattering

PACS number(s): 71.55.Ak, 25.40.Fq, 75.30.Ds, 75.50.Gg

Citation: C. Liu, J. L. Shen, J. C. Gao, C. J. Yi, D. Liu, T. Xie, L. Yang, S. Danilkin, G. C. Deng, W. H. Wang, S. L. Li, Y. G. Shi, H. M. Weng, E. K. Liu, and H. Q. Luo, Spin excitations and spin wave gap in the ferromagnetic Weyl semimetal $Co_3Sn_2S_2$, Sci. China-Phys. Mech. Astron. **64**, 217062 (2021), https://doi.org/10.1007/s11433-020-1597-6

1 Introduction

Magnetic topological materials, which combine non-trivial band topology and magnetic order, have significant potential for fundamental physics and technology applications. This promise stems from a number of exotic quantum phenomena including the quantum anomalous Hall effect, topological axion state, and chiral Majorana fermions, etc [1-6]. In recent years, an increasing number of intrinsic magnetic materials has been theoretically predicted as magnetic Dirac semimetals (DSMs), Weyl semimetals (WSMs), and topological insulators (TIs) [7-14]. Although a few of these materials have been experimentally confirmed [15-24], their spin dynamics and the interplay with topological electron states remain unclear [25, 26].

Specifically in ferromagnetic WSMs, the Weyl nodes serve as the magnetic monopoles of the Berry curvature, which

*Corresponding authors (HongMing Weng, email: hmweng@iphy.ac.cn; EnKe Liu, email: ekliu@iphy.ac.cn; HuiQian Luo, email: hqluo@iphy.ac.cn)
† These authors contributed equally to this work.

leads to the intrinsic anomalous Hall effect (AHE) in the bulk transport properties [27-29]. Moreover, these Weyl nodes can also affect the spin wave dispersions, since the spin operators and the current operators around these nodes are in one-to-one correspondence, leading to a direct connection between spin dynamics and AHE [30,31]. For example, in a magnetic WSM candidate $SrRuO_3$, the impact of Weyl points induces a non-monotonic temperature dependence of the anomalous Hall conductivity (AHC) $\sigma_{xy}(T)$, which is manifested in both the spin wave gap E_g and its stiffness D [31,32]. Such results are distinct from those obtained for the conventional ferromagnetic metals. The spin waves of ferromagnetic metals are usually either gapless in the weak correlation limit, or show a monotonic spin gap following the magnetic order parameter in the strong correlation limit with spin-orbit coupling (SOC) [30]. Investigations on the energy dependence of spin excitations below and above the Curie temperature (T_C) can provide important information about the spin-spin interactions and correlations regarding their crucial role in the AHE.

$Co_3Sn_2S_2$ is a new experimentally verified ferromagnetic WSM with very promising topological properties [17-21]. This material is a Shandite compound characterized by a rhombohedral structure (space group: $R\bar{3}m$) with quasi-two-dimensional (quasi-2D) Co_3Sn layers sandwiched between S atoms [33, 34]. The magnetic Co atoms arrange on a kagome lattice in the ab-plane with ~0.3μ_B/Co ordered moments aligned along the c-axis below T_C = 177 K (Figure 1(a)) [35-37]. There are three pairs of Weyl nodes in the first Brillouin zone close to the Fermi level (Figure 1(b)), as evidenced by the surface Fermi-arcs and linear bulk band dispersions observed from spectroscopic experiments [11, 17-20]. With the considerably enhanced Berry curvature from its band structure (Figure 1(c)), a record of large AHC is detected up to 1130 Ω^{-1}cm^{-1} accompany by a strong temperature dependence approaching T_C [17,38].

In this paper, we report a comprehensive neutron scattering study on the $Co_3Sn_2S_2$ single crystals, where the spin excitations up to 18 meV both in the ferromagnetic and paramagnetic states are measured. Both in-plane and out-of-plane dispersions are found, suggesting that the magnetic interactions are actually three-dimensional (3D) in despite of its quasi-2D lattice structure. The paramagnetic excitations above T_C (T = 200 K) exhibit similar dispersions but damped intensities. Theoretical calculations on the effective exchange couplings correspond closely to the experimental T_C and large spin stiffness. However, the magnetic anisotropy energy (~0.6 meV) is considerably smaller than the spin wave gap E_g =2.3 meV observed at T = 4 K. Further analysis on the temperature dependence of the gap suggests a significant contribution from AHC. Therefore, $Co_3Sn_2S_2$ is a moderately correlated ferromagnet, where the conducting electrons related to Weyl fermions are deeply involved into its spin dynamics.

2 Experimental method

We prepared high-quality $Co_3Sn_2S_2$ single crystals using a previously reported flux method (See Supplemental Materials). The zero-field-cooling magnetization and resistivity reveal a clear ferromagnetic transition at T_C = 174 K, and another anomaly at T_A = 136 K (Figure 1(d) and (e)), which may be related to the formation of an in-plane antiferromagnetic order [39,40]. The extremely large anisotropy of magnetization between $B \parallel c$ and $B \parallel ab$ geometry confirms the c-axis polarized magnetism [35-37]. Neutron scattering experiments were performed using a thermal triple-axis spectrometer (Taipan) and a cold triple-axis spectrometer (Sika) at Australian Centre for Neutron Scattering, ANSTO, Australia [41, 42]. For Taipan experiments, the final neutron

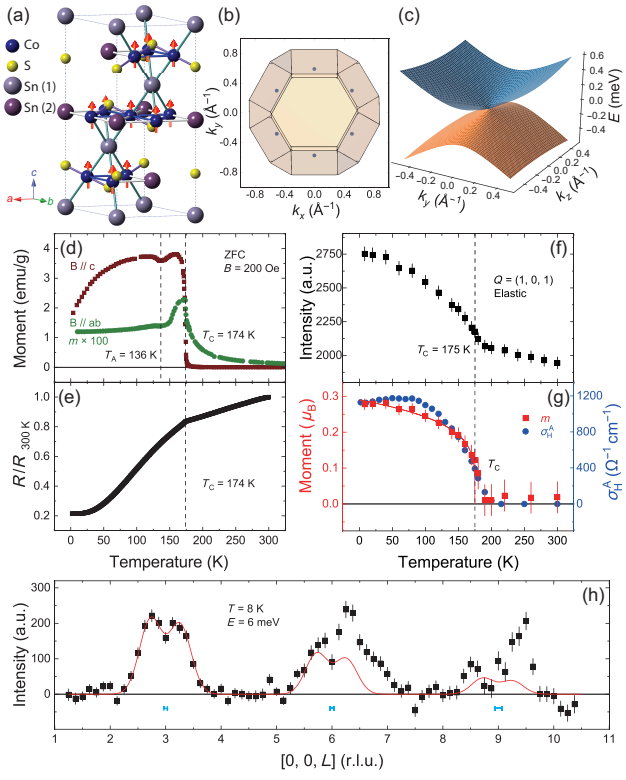

Figure 1 (Color online) (a) Crystal and magnetic structure of $Co_3Sn_2S_2$. (b) The location of Weyl points in the Brillouin zone along the z axis. (c) Dispersion of the Weyl Hamiltonian on the k_x = 0 plane. (d), (e) Temperature dependence of the magnetization and resistivity. (f), (g) Temperature dependence of the peak intensity at Q = (1, 0, 1), and the deduced ordered moment m compared with the anomalous Hall conductivity σ_H^A. (h) Spin excitations at 6 meV along $\mathbf{Q}$ = [0, 0, L] direction. The red lines represent two Gaussian-fittings based on L = 3 data, which are normalized by the magnetic form factor for L = 6 and 9. The horizontal bars indicate the calculated instrument resolution.

energy was fixed to E_f = 14.87 meV, using a pyrolytic graphite filter, double focusing monochromator, and vertical focusing analyzer. Approximately 1.5 gram single crystals of $Co_3Sn_2S_2$ were co-aligned with a hydrogen-free glue on several thin aluminum plates. For Sika experiments, a final energy of E_f = 5 meV was set using a cooled Be filter, double focusing monochromator, and flat analyzer. A large piece of single crystal (mass: ~7.6 g) was used. We defined the scattering plane $[H, 0, 0] \times [0, 0, L]$ using hexagonal unit cell where $a = b = 5.352$ Å, $c = 13.095$ Å, $\alpha = \beta = 90°$, $\gamma = 120°$, and $\mathbf{Q} = H\mathbf{a}^* + K\mathbf{b}^* + L\mathbf{c}^*$, where H, K, and L are Miller indices. Thus the d-spacing is determined from ref. [43]: $d_{HKL} = 1/\sqrt{4(H^2 + HK + K^2)/3a^2 + L^2/c^2}$. The instrument resolution is calculated by ResLib [44].

3 Results and discussion

3.1 Magnetic order parameter

We have first performed elastic neutron scattering measurements on a Bragg peak at Q = (1, 0, 1), where the nuclear scattering is weak. The integrated intensity of the (1, 0, 1) peak reveals a clear ferromagnetic transition at T_C = 175 K, consistent with the magnetization results (Figure 1(f)). The ordered moment M can be estimated by comparing the intensities associated with magnetic scattering and nuclear scattering [45] (See Supplemental Materials). A value of $0.28 \pm 0.02\,\mu_B$ per Co atom at the base temperature of T =8 K was obtained. The weak ordered moment is consistent with previous findings report on powder neutron diffraction experiments [35] and reflects its itinerant and semi-metallic character, where both holes and electrons contribute to the Fermi surfaces [11, 17, 18]. The magnetic order parameter $M(T)$ follows similar temperature dependence as AHC, except for a discrepancy from T = 50 K to 150 K. This results from the fact that the intrinsic AHC is mainly determined by the Berry curvature at low temperatures away from T_C (Figure 1(g)) [17]. A critical exponent β of 0.21 ± 0.04 is determined by fitting the magnetic order parameter using $M(T) = M_0(1 - T/T_C)^{\beta}$ for a second-order magnetic transition (red line in Figure 1(g)).

3.2 Low-energy spin waves

Neutron scattering is unable to reach the primary ferromagnetic excitations centering around Q = 0 at a finite energy transfer [46]. Therefore, we instead seek the magnetic excitation signal along $Q = (0, 0, L)$, and measure the background at $Q = (\pm 0.3, 0, L)$ or $(\pm 0.5, 0, L)$ at identical energies. Figure 1(h) shows a typical constant-energy scan at E = 6 meV and T =8 K. Local signals emerge only at $L = 3, 6, 9$ with two splitting incommensurate peaks, where signals at high Q are contaminated by the phonon scattering from $Co_3Sn_2S_2$ samples and the aluminium sample holder. We have further mapped out the spin waves via constant-energy scans from E = 2 meV to 18 meV along both $[H, 0, 3]$ and $[0, 0, L]$ directions at T =8 K (Figure 2(a) and (b)). Peaks centering $Q = (0, 0, 3)$ both along the H and L directions at 2 meV are absent. Therefore, we consider (in general) a full spin wave gap below 2 meV even if the gap cuts the resolution edge of a thermal triple-axis spectrometer. Above 2 meV, a steep dispersion of the in-plane spin waves along the H direction is observed, while the out-of-plane spin waves along the L direction are quite dispersive and broad in peak width. Phonon signals also show up outside the spin wave branches around 16 meV (See Supplemental Materials). By warming up to the paramagnetic state at T = 200 K, the spin excitations above 8 meV are heavily damped, and the strength of the low-energy spin excitations below 4 meV increases, as the gap is closed (Figure 2(c) and (d)). To qualitatively compare

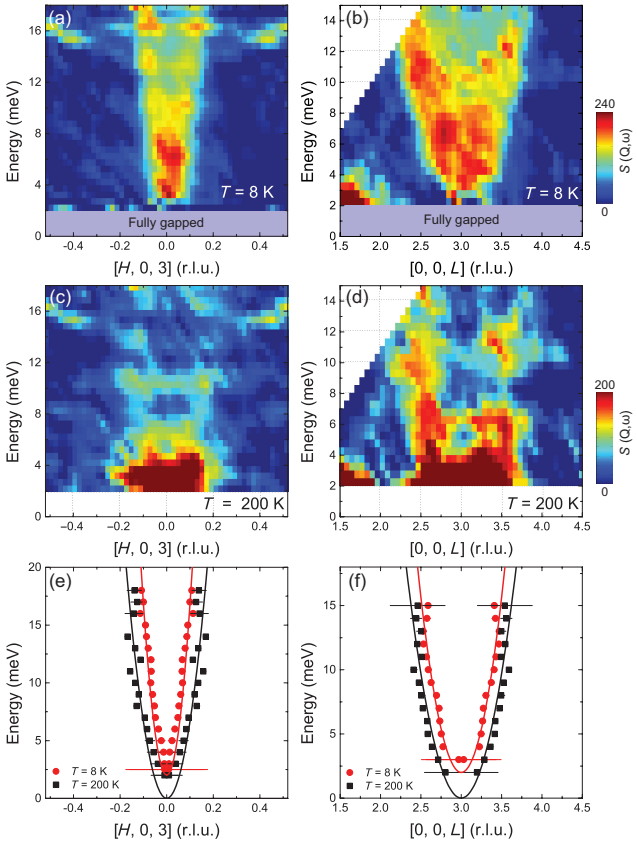

Figure 2 (Color online) (a)-(d) In-plane and out-of-plane spin waves at T = 8 K and paramagnetic excitations at T = 200 K around Q = (0, 0, 3). The high energy data at low Q side in panel (c) and (d) are missing due to scattering restrictions, and strong contaminations from quasi-elastic scattering prevent measurements of data below 2 meV. (e), (f) Dispersion of the spin excitations obtained from two Gaussian-fittings of the raw data. The solids lines are fitting results with q^2-dependence.

the dispersion below and above T_C, we performed two Gaussian-fittings on the raw data after the relevant background subtraction (See Supplemental Materials). Owing to scattering restrictions, we are unable to reach the band top at the zone boundary, hence, full fitting based on a microscopic model of spin waves is impossible from these limited data. However, we can still roughly fit the dispersion at 8 K with the q^2-dependence: $E = E_g + Dq^2$ (assuming E_g=2 meV), where $D \sim S|J|$ represents the spin stiffness in a ferromagnetic system with exchange coupling J and effective spin S (Figure 2(e) and (f)) [47]. The spin excitations at 200 K are gapless and can be also fitted by the same equation (here E_g=0 meV), but with smaller D than the case below T_C. The fitting results of D (see Table 1) reveal that, in both the ferromagnetic and paramagnetic states, D is considerably larger than that reported in $SrRuO_3$ case [31,32].

3.3 Theoretical calculations

The $Co_3Sn_2S_2$ compound is considered as an itinerant ferromagnet below T_C [17, 18]. However, we can still estimate the effective exchange couplings by viewing the ordered moments located on Co sites and then calculating the total energy variation for small deviations of ground state magnetic configuration. A semi-classical model analogous to the Heisenberg Hamiltonian can be expressed as:

$$H = \sum_{<i,j>} J_{ij}\mathbf{e}_i\mathbf{e}_j, \tag{1}$$

where $\mathbf{e}_{i,j}$ are unit vectors that point to the direction of the spin $S_{i,j}$, and J_{ij} denotes the exchange coupling between the ith and jth sites, as shown in Figure 3(a). Thus, we can define the total exchange interactions between a central Co atom and all its neighbors, up to quite long range where the exchange interaction is zero: $J_0 = \sum_i J_{0i}$. The spin interactions between one and 400 neighboring Co atoms were calculated using a multiple-scattering Green function method [48]. This yielded values of $J_1 = -2.37$ meV, $J_2 = -0.16$ meV, $J_3 = -0.02$ meV, $J_{c1} = -0.30$ meV, $J_{c2} = -0.75$ meV, and $J_{c3} = -0.11$ meV (See Supplemental Materials, here we assume the effective spin S=1). Admittedly, such calculations are highly model dependent, however, the calculated results can be verified by the experimental data. First, the Curie temperature is determined as follows: $T_C = 2J_0\langle M^2\rangle/3k_B\langle M\rangle^2$, where $\langle M^2\rangle/\langle M\rangle^2 = 1$ for a classical ferromagnetic system [49]. We evaluate $T_C = 2J_0/3k_B = 167$ K, which is fairly close to the experimental value (175 K). Second, the spin stiffness tensor is determined as bellow:

$$D_{\alpha\beta} = \frac{2}{M}\sum_j J_{0j}R_{j\alpha}R_{j\beta}, \tag{2}$$

where $R_{j\alpha}$ denotes the α-direction component of the lattice vector $\mathbf{R}_j$. Using the above J_{ij}, we calculated the in-plane spin stiffness and the obtained value agrees with experimental data, although the out-of-plane spin stiffness may be over estimated in such a local moment picture (Table 1). Third, the comparable exchange couplings for out-of-plane (J_{ci}) and in-plane ($J_{1,2}$) also support the 3D spin waves, since the locations of ordered moments in Co chains along the c-axis are shifted along the a-axis for the adjacent kagome layers (Figure 1(a)). We summed over all contributions from the atoms located the same distance from the central Co atom. For both in-plane and out-of-plane spin interactions, an effective distance of ~12 Å was found, suggesting most of the interactions from the nearest spins in the Co kagome unit (Figure 3(b)). Finally, we estimate the spin anisotropy energy by calculating the energy difference when all the local moments are rotated from the ground state to the same angle within the *xoz* plane or *xoy* plane. The maximum energy obtained between two geometries (~0.6 meV) is consistent with the magnetization results (inset of Figure 3(b)) [17,50].

3.4 Spin wave gaps

The 3D spin interactions persisting both below and above T_C with large stiffness suggest that $Co_3Sn_2S_2$ has a moderate correlation and strong itinerancy for supporting the dispersive excitations against temperature. Hence, the Weyl fermions associated with the conduct electrons will probably contribute to the low-energy spin excitations. Measurements of the temperature-dependent dispersions of the spin waves

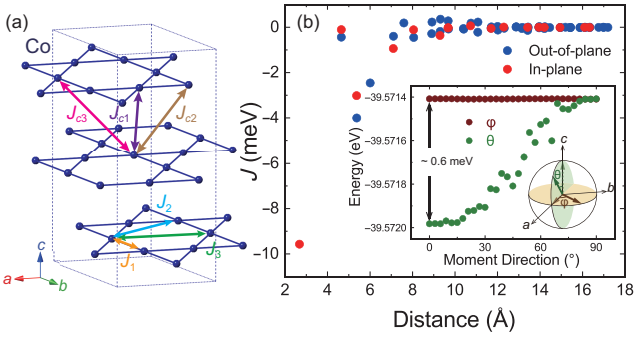

Figure 3 (Color online) (a) Effective exchange interactions between Co atoms in our first principle calculations. (b) Estimation of the effective correlation length of the exchange interactions (main panel) and the total energy of the moment rotation (inset) for both in-plane and out-of-plane cases.

Table 1 Experimental and calculated results of D and T_C

Experiment	D_H(8 K) (meVÅ^2)	D_L(8 K) (meVÅ^2)	D_H(200 K) (meVÅ^2)	D_L(200 K) (meVÅ^2)
Value	803 ± 46	237 ± 13	360 ± 30	169 ± 10
Calculation	D_{xx} (meVÅ^2)	D_{yy} (meVÅ^2)	D_{zz} (meVÅ^2)	T_C (K)
Value	945	833	656	167

are extremely time consuming in triple-axis neutron experiments and, therefore, we map out the spin wave gap below T_C instead. As shown in Figure 4(a), compared with the case of $T = 200$ K and 300 K data, with an energy resolution of $\Delta E = 1{\sim}2$ meV, the spin wave gap yields a clear reduction in spin excitation intensity below 4 meV for $T = 8$ K. For measurements under relatively high resolution ($\Delta E \approx 0.1$ meV), the spin wave gap is precisely determined as a full gap below 2.3 meV at $T = 4$ K (Figure 4(b)), where there is no excitation signal at $E = 2$ meV, but a tiny peak occurs at E=2.5 meV (Figure 4(c)). The gap closes gradually during warming up and disappears completely above T_C (Figure 4(b)-(e)), giving rise to a well-defined Gaussian peak at $E = 0.3$ meV and $T = 175$ K (Figure 4(d)). The spin wave gap is considerably larger than the estimated spin anisotropy energy, owing possible contributions from the Weyl fermions.

Theoretically, the spin wave gap in magnetic WSMs at $q = 0$ is given by $E_g = \mathcal{K}/\alpha$, where the coefficient α represents the Berry phase term and $\mathcal{K}$ measures the spin anisotropy energy from SOC [31] (See Supplemental Materials). α has two contributions: one is $\alpha_0 = c_0/\langle S^z\rangle$ from the finite contribution without SOC, and the other is $\alpha_1 = \lambda\sigma_{xy}$,

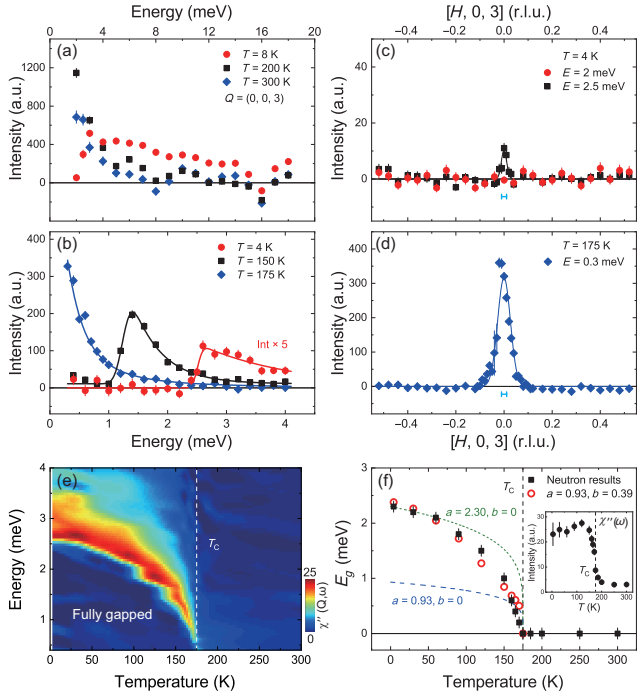

Figure 4 (Color online) (a) Energy dependence of the spin excitations at $T = 8$, 200, and 300 K measured at Taipan. (b) High resolution energy dependence of the spin excitations at $T = 4$, 150, and 175 K measured at Sika. (c), (d) Constant-energy scans for $E = 2$ and 2.5 meV at $T = 4$ K, and $E = 0.3$ meV at $T = 175$ K. The solid lines are Gaussian fittings, and the horizontal bars indicate the instrument resolution. (e) Temperature dependence of the spin dynamic susceptibility $\chi''(Q,\omega)$ at low energy. (f) Temperature dependence of the spin wave gap and fitting results by eq. (2) with different parameters. Inset shows the integral intensity $\chi''(\omega)$ up to 4 meV.

which results from the existence of Weyl nodes and is directly related to σ_{xy} [31]. The parameter λ is determined by the shape of Weyl cones. By introducing the normalization factors M_0 (saturated moment) and $\sigma_0 = e^2/ha_0$ (a_0 is the lattice constant), the temperature dependence of E_g can be described by the following phenomenological equation:

$$E_g(T) = \frac{aM(T)/M_0}{1 + b(M(T)/M_0)(\sigma_{xy}(T)/\sigma_0)}, \tag{3}$$

where $a = \mathcal{K}\langle S^z\rangle_0/c_0$ and $b = \lambda\sigma_0\langle S^z\rangle_0/c_0$ are nearly temperature independent constants. Therefore, with the contribution from Weyl fermions ($b \neq 0$), $E_g(T)$ probably deviates from the behavior of the magnetic order parameter $M(T)$ for the involvement of $\sigma_{xy}(T)$. The temperature dependence of the gap seems to have an order-parameter-like behavior, accompanied by an abrupt decrease above T_C for the integrated dynamic susceptibility χ'' from E_g to 4 meV (inset of Figure 4(f)). However, the direct fitting based on $E_g(T) = E_0(1 - T/T_C)^\beta$ would yield an unreasonable critical exponent $\beta = 0.53$ with a large discrepancy for $\beta = 0.21$ deduced from the actual order parameter in Figure 1(g). A full description of $E_g(T)$ either by using fixed $\beta = 0.21$, while ignoring the contribution from Weyl fermions, as shown by the green dash line in Figure 4(f) (namely, $a = 2.30$ meV and $b = 0$ in eq. (3)) is impossible. The $E_g(T)$ is well reproduced only when we consider the involvement of σ_{xy} (which is $-\sigma_H^A$ in Figure 1(g)), as shown by the open circles in Figure 4(f), thus we have $a = 0.93$ meV and $b = 0.39$ in eq. (3). For comparison, the parameters $a = 0.93$ meV and $b = 0$ are also failed to fit the results, thereby confirming the strong interplay between the Weyl topology and the spin dynamics. Notably, the coefficient b here in $Co_3Sn_2S_2$ is positive and thus opposite to the case of $SrRuO_3$ with $b = -9.5$ or -4.98 (assuming σ_{xy} is negative) [31,32], which depends on the detailed shapes of Weyl cones in these two compounds.

4 Conclusions

In summary, we have performed neutron scattering experiments on the recently verified magnetic WSM $Co_3Sn_2S_2$. In contrast to its quasi-2D lattice structure, the spin excitations both in the ferromagnetic and paramagnetic states are revealed with 3D characters. Theoretical calculations suggest comparable in-plane and out-of-plane magnetic exchange interactions, further estimation is consistent with the experimental T_C and large spin stiffness. We have precisely determined a full spin wave gap and its temperature dependence below T_C, which is much larger than the spin anisotropy energy and certainly affected by the AHC triggered by the Weyl fermions. Our results give basic knowledge about the spin

dynamics in $Co_3Sn_2S_2$ and solid evidences about how it interplays with the topological electron states.

This work was supported by the National Key Research and Development Program of China (Grant Nos. 2017YFA0303100, 2017YFA0302900, 2016YFA0300500, 2017YFA0206300, and 2019YFA0704900), the National Natural Science Foundation of China (Grant Nos. 11974392, 11974394, 11822411, 51722106, 11674372, 11774399, 11961160699, and 12061130200), the Strategic Priority Research Program (B) of the Chinese Academy of Sciences (CAS) (Grant Nos. XDB07020300, XDB25000000, and XDB33000000), and the Beijing Natural Science Foundation (Grant Nos. JQ19002, Z180008, and Z190009). EnKe Liu and HuiQian Luo are grateful for the support from the Youth Innovation Promotion Association of CAS (Grant Nos. 2013002, and 2016004). HongMing Weng thanks the support from the K. C. Wong Education Foundation (GJTD-2018-01).

Supporting Information

The supporting information is available online at phys.scichina.com and link.springer.com. The supporting materials are published as submitted, without typesetting or editing. The responsibility for scientific accuracy and content remains entirely with the authors.

1 B. Yan, and C. Felser, Annu. Rev. Condens. Matter Phys. **8**, 337 (2017), arXiv: 1611.04182.
2 Y. Tokura, K. Yasuda, and A. Tsukazaki, Nat. Rev. Phys. **1**, 126 (2019).
3 J. Zou, Z. He, and G. Xu, npj Comput. Mater. **5**, 96 (2019), arXiv: 1909.11999.
4 H. Weng, R. Yu, X. Hu, X. Dai, and Z. Fang, Adv. Phys. **64**, 227 (2015), arXiv: 1508.02967.
5 C. Shekhar, A. K. Nayak, Y. Sun, M. Schmidt, M. Nicklas, I. Leermakers, U. Zeitler, Y. Skourski, J. Wosnitza, Z. Liu, Y. Chen, W. Schnelle, H. Borrmann, Y. Grin, C. Felser, and B. Yan, Nat. Phys. **11**, 645 (2015), arXiv: 1502.04361.
6 Q. L. He, L. Pan, A. L. Stern, E. C. Burks, X. Che, G. Yin, J. Wang, B. Lian, Q. Zhou, E. S. Choi, K. Murata, X. Kou, Z. Chen, T. Nie, Q. Shao, Y. Fan, S. C. Zhang, K. Liu, J. Xia, and K. L. Wang, Science **357**, 294 (2017), arXiv: 1606.05712.
7 H. Chen, Q. Niu, and A. H. MacDonald, Phys. Rev. Lett. **112**, 017205 (2014), arXiv: 1309.4041.
8 P. Tang, Q. Zhou, G. Xu, and S. C. Zhang, Nat. Phys. **12**, 1100 (2016), arXiv: 1603.08060.
9 Z. Wang, M. G. Vergniory, S. Kushwaha, M. Hirschberger, E. V. Chulkov, A. Ernst, N. P. Ong, R. J. Cava, and B. A. Bernevig, Phys. Rev. Lett. **117**, 236401 (2016), arXiv: 1603.00479.
10 G. Chang, S. Y. Xu, H. Zheng, B. Singh, C. H. Hsu, G. Bian, N. Alidoust, I. Belopolski, D. S. Sanchez, S. Zhang, H. Lin, and M. Z. Hasan, Sci. Rep. **6**, 38839 (2016), arXiv: 1603.01255.
11 Q. Xu, E. Liu, W. Shi, L. Muechler, J. Gayles, C. Felser, and Y. Sun, Phys. Rev. B **97**, 235416 (2018), arXiv: 1801.00136.
12 G. Hua, S. Nie, Z. Song, R. Yu, G. Xu, and K. Yao, Phys. Rev. B **98**, 201116(R) (2018), arXiv: 1801.02806.
13 Y. Shi, J. Kahn, B. Niu, Z. Fei, B. Sun, X. Cai, B. A. Francisco, D. Wu, Z. X. Shen, X. Xu, D. H. Cobden, and Y. T. Cui, Sci. Adv. **5**, eaat8799 (2019), arXiv: 1807.09342.
14 D. Zhang, M. Shi, T. Zhu, D. Xing, H. Zhang, and J. Wang, Phys. Rev. Lett. **122**, 206401 (2019), arXiv: 1808.08014.
15 J. Y. Liu, J. Hu, Q. Zhang, D. Graf, H. B. Cao, S. M. A. Radmanesh, D. J. Adams, Y. L. Zhu, G. F. Cheng, X. Liu, W. A. Phelan, J. Wei, M. Jaime, F. Balakirev, D. A. Tennant, J. F. DiTusa, I. Chiorescu, L. Spinu, and Z. Q. Mao, Nat. Mater. **16**, 905 (2017), arXiv: 1507.07978.
16 L. Ye, M. Kang, J. Liu, F. von Cube, C. R. Wicker, T. Suzuki, C. Jozwiak, A. Bostwick, E. Rotenberg, D. C. Bell, L. Fu, R. Comin, and J. G. Checkelsky, Nature **555**, 638 (2018), arXiv: 1709.10007.
17 E. Liu, Y. Sun, N. Kumar, L. Muechler, A. Sun, L. Jiao, S. Y. Yang, D. Liu, A. Liang, Q. Xu, J. Kroder, V. Süβ, H. Borrmann, C. Shekhar, Z. Wang, C. Xi, W. Wang, W. Schnelle, S. Wirth, Y. Chen, S. T. B. Goennenwein, and C. Felser, Nat. Phys. **14**, 1125 (2018), arXiv: 1712.06722.
18 Q. Wang, Y. Xu, R. Lou, Z. Liu, M. Li, Y. Huang, D. Shen, H. Weng, S. Wang, and H. Lei, Nat. Commun. **9**, 3681 (2018), arXiv: 1712.09947.
19 D. F. Liu, A. J. Liang, E. K. Liu, Q. N. Xu, Y. W. Li, C. Chen, D. Pei, W. J. Shi, S. K. Mo, P. Dudin, T. Kim, C. Cacho, G. Li, Y. Sun, L. X. Yang, Z. K. Liu, S. S. P. Parkin, C. Felser, and Y. L. Chen, Science **365**, 1282 (2019), arXiv: 1909.09580.
20 N. Morali, R. Batabyal, P. K. Nag, E. Liu, Q. Xu, Y. Sun, B. Yan, C. Felser, N. Avraham, and H. Beidenkopf, Science **365**, 1286 (2019), arXiv: 1903.00509.
21 H. M. Weng, Sci. China-Phys. Mech. Astron. **62**, 127031 (2019).
22 I. Belopolski, K. Manna, D. S. Sanchez, G. Chang, B. Ernst, J. Yin, S. S. Zhang, T. Cochran, N. Shumiya, H. Zheng, B. Singh, G. Bian, D. Multer, M. Litskevich, X. Zhou, S. M. Huang, B. Wang, T. R. Chang, S. Y. Xu, A. Bansil, C. Felser, H. Lin, and M. Z. Hasan, Science **365**, 1278 (2019), arXiv: 2004.00004.
23 M. M. Otrokov, I. I. Klimovskikh, H. Bentmann, D. Estyunin, A. Zeugner, Z. S. Aliev, S. Gaβ, A. U. B. Wolter, A. V. Koroleva, A. M. Shikin, M. Blanco-Rey, M. Hoffmann, I. P. Rusinov, A. Y. Vyazovskaya, S. V. Eremeev, Y. M. Koroteev, V. M. Kuznetsov, F. Freyse, J. Sánchez-Barriga, I. R. Amiraslanov, M. B. Babanly, N. T. Mamedov, N. A. Abdullayev, V. N. Zverev, A. Alfonsov, V. Kataev, B. Büchner, E. F. Schwier, S. Kumar, A. Kimura, L. Petaccia, G. Di Santo, R. C. Vidal, S. Schatz, K. Kiβner, M. Ünzelmann, C. H. Min, S. Moser, T. R. F. Peixoto, F. Reinert, A. Ernst, P. M. Echenique, A. Isaeva, and E. V. Chulkov, Nature **576**, 416 (2019), arXiv: 1809.07389.
24 Y. Deng, Y. Yu, M. Z. Shi, Z. Guo, Z. Xu, J. Wang, X. H. Chen, and Y. Zhang, Science **367**, 895 (2020), arXiv: 1904.11468.
25 P. Park, J. Oh, K. Uhlířová, J. Jackson, A. Deák, L. Szunyogh, K. H. Lee, H. Cho, H. L. Kim, H. C. Walker, D. Adroja, V. Sechovský, and J. G. Park, npj Quant. Mater. **3**, 63 (2018), arXiv: 1811.07549.
26 S. Itoh, Y. Endoh, T. Yokoo, D. Kawana, Y. Kaneko, Y. Tokura, and M. Fujita, J. Phys. Soc. Jpn. **82**, 043001 (2013), arXiv: 1209.1780.
27 F. D. M. Haldane, Phys. Rev. Lett. **93**, 206602 (2004), arXiv: cond-mat/0408417.
28 D. Xiao, M. C. Chang, and Q. Niu, Rev. Mod. Phys. **82**, 1959 (2010), arXiv: 0907.2021.
29 A. A. Burkov, Phys. Rev. Lett. **113**, 187202 (2014), arXiv: 1406.3033.
30 M. Onoda, A. S. Mishchenko, and N. Nagaosa, J. Phys. Soc. Jpn. **77**, 013702 (2008).
31 S. Itoh, Y. Endoh, T. Yokoo, S. Ibuka, J. G. Park, Y. Kaneko, K. S. Takahashi, Y. Tokura, and N. Nagaosa, Nat. Commun. **7**, 11788 (2016).
32 K. Jenni, S. Kunkemöller, D. Brüning, T. Lorenz, Y. Sidis, A. Schneidewind, A. A. Nugroho, A. Rosch, D. I. Khomskii, and M. Braden, Phys. Rev. Lett. **123**, 017202 (2019), arXiv: 1902.04036.
33 R. Weihrich, I. Anusca, and M. Zabel, Z. Anorg. Allg. Chem. **631**, 1463 (2005).
34 R. Weihrich, and I. Anusca, Z. Anorg. Allg. Chem. **632**, 1531 (2006).
35 P. Vaqueiro, and G. G. Sobany, Solid State Sci. **11**, 513 (2009).
36 W. Schnelle, A. Leithe-Jasper, H. Rosner, F. M. Schappacher, R. Pöttgen, F. Pielnhofer, and R. Weihrich, Phys. Rev. B **88**, 144404

(2013).
37 M. A. Kassem, Y. Tabata, T. Waki, and H. Nakamura, J. Phys. Soc. Jpn. **85**, 064706 (2016).
38 R. Yang, T. Zhang, L. Zhou, Y. Dai, Z. Liao, H. Weng, and X. Qiu, Phys. Rev. Lett. **124**, 077403 (2020), arXiv: 1908.03895.
39 M. A. Kassem, Y. Tabata, T. Waki, and H. Nakamura, Phys. Rev. B **96**, 014429 (2017), arXiv: 1702.05627.
40 Z. Guguchia, J. A. T. Verezhak, D. J. Gawryluk, S. S. Tsirkin, J. X. Yin, I. Belopolski, H. Zhou, G. Simutis, S. S. Zhang, T. A. Cochran, G. Chang, E. Pomjakushina, L. Keller, Z. Skrzeczkowska, Q. Wang, H. C. Lei, R. Khasanov, A. Amato, S. Jia, T. Neupert, H. Luetkens, and M. Z. Hasan, Nat. Commun. **11**, 559 (2020).
41 S. A. Danilkin, and M. Yethiraj, Neutron. News. **20**, 37 (2009).
42 C. M. Wu, G. Deng, J. S. Gardner, P. Vorderwisch, W. H. Li, S. Yano, J. C. Peng, and E. Imamovic, J. Inst. **11**, P10009 (2016).
43 G. Wang, and T. Lu, *RHEED Transmission Mode and Pole Figures* (Springer, New York, 2014), pp.7-22.
44 E. Farhi, Y. Debab, and P. Willendrup, J. Neut. Res. **17**, 5 (2013).
45 D. Gong, T. Xie, R. Zhang, J. Birk, C. Niedermayer, F. Han, S. H. Lapidus, P. Dai, S. Li, and H. Luo, Phys. Rev. B **98**, 014512 (2018), arXiv: 1807.01612.
46 J. Van Kranendonk, and J. H. Van Vleck, Rev. Mod. Phys. **30**, 1 (1958).
47 D. Price, and F. Fernandez-Alonso, *Neutron Scattering-Magnetic and Quantum Phenomena* (Elsevier, London, 2015).
48 D. M. Korotin, V. V. Mazurenko, V. I. Anisimov, and S. V. Streltsov, Phys. Rev. B **91**, 224405 (2015), arXiv: 1411.4169.
49 A. I. Liechtenstein, M. I. Katsnelson, V. P. Antropov, and V. A. Gubanov, J. Magn. Magn. Mater. **67**, 65 (1987).
50 J. Shen, Q. Zeng, S. Zhang, W. Tong, L. Ling, C. Xi, Z. Wang, E. Liu, W. Wang, G. Wu, and B. Shen, Appl. Phys. Lett. **115**, 212403 (2019), arXiv: 2002.03940.